

JPSS-1 VIIRS Pre-Launch Radiometric Performance

Hassan Oudrari^a, Jeff McIntire^a, Xiaoxiong Xiong^b, James Butler^b, Qiang Ji^a, Tom Schwarting^a, and Jinan Zeng^c,

^aScience Systems and Applications Incorporation, Lanham, MD, 20706 USA

^bNASA Goddard Space Flight Center, Greenbelt, MD, 20771 USA.

^cFibertek Inc, Herndon, VA, 20171

ABSTRACT

The first Joint Polar Satellite System (JPSS-1 or J1) mission is scheduled to launch in January 2017, and will be very similar to the Suomi-National Polar-orbiting Partnership (SNPP) mission. The Visible Infrared Imaging Radiometer Suite (VIIRS) on board the J1 spacecraft completed its sensor level performance testing in December 2014. VIIRS instrument is expected to provide valuable information about the Earth environment and properties on a daily basis, using a wide-swath (3,040 km) cross-track scanning radiometer. The design covers the wavelength spectrum from reflective to long-wave infrared through 22 spectral bands, from 0.412 μm to 12.01 μm , and has spatial resolutions of 370 m and 740 m at nadir for imaging and moderate bands, respectively. This paper will provide an overview of pre-launch J1 VIIRS performance testing and methodologies, describing the at-launch baseline radiometric performance as well as the metrics needed to calibrate the instrument once on orbit. Key sensor performance metrics include the sensor signal to noise ratios (SNRs), dynamic range, reflective and emissive bands calibration performance, polarization sensitivity, bands spectral performance, response-vs-scan (RVS), near field response, and stray light rejection. A set of performance metrics generated during the pre-launch testing program will be compared to the sensor requirements and to SNPP VIIRS pre-launch performance.

Keywords: JPSS, VIIRS, Radiometric, Reflective, Emissive, Calibration, Performance

1. INTRODUCTION

The Visible and Infrared Imaging Radiometer Suite (VIIRS) is a multi-spectral electro-optical imager designed to observe the Earth from a satellite in a circular orbit with nominal altitude of 828 km. The first VIIRS is being carried on the Suomi-National Polar-orbiting Partnership (SNPP) satellite (launched on October 28, 2011) and future builds will be aboard all satellites of the Joint Polar Satellite System (JPSS). All these satellites will be in a sun-synchronous orbits inclined 8.7 degrees from the poles. The VIIRS data will be critical to the generation of more than 22 Environmental Data Records (EDRs) used by NOAA, NASA, and scientific users. As VIIRS orbits, it observes a swath of Earth over 3,000 km wide centered on the sub-satellite track. This width is sufficient that VIIRS images every point of the Earth's surface twice every 24 hours (once in daylight and once at night).

J1 VIIRS performance results presented in this paper are based on the test data analysis executed by the NASA VIIRS Characterization Support Team (VCST), with close collaboration with other teams, including the National Aeronautics and Space Administration (NASA), the Aerospace Corporation, the National Oceanic and Atmospheric Administration (NOAA), the University of Wisconsin and Raytheon company. VIIRS instrument design is based on a scanning radiometer that collects imagery and radiometric measurements of Earth's surface to study land, atmosphere, oceans and clouds. These data are used in the operational processing to generate environmental data in support of data continuity initiated by heritage sensors such as the Advanced Very High Resolution Radiometer (AVHRR), the Sea-viewing Wide Field-of-view Sensor (SeaWiFS) and the Moderate Resolution Imaging Spectroradiometer (MODIS). VIIRS data products are being used in weather forecasting, and global measurements of atmospheric, oceanic, and land surface variables.¹

Sections 2 of this paper will provide an overview of J1 VIIRS hardware design and pre-launch radiometric and spectral performance testing and requirements. The summary of VIIRS pre-launch testing and sensor performance will be presented in Section 3 for all Reflective Solar Bands (RSB) and Thermal Emissive Bands (TEB) calibration (beginning of life performance), focusing on key performance metrics such as the signal-to-noise (SNR), dynamic range, polarization, radiometric calibration uncertainties, relative spectral response and scattered light contamination. Section 4 will present a summary and conclusion of J1 VIIRS pre-launch radiometric and spectral performance as well as future performance enhancements.

2. VIIRS HARDWARE DESIGN AND PERFORMANCE TESTING

2.1 Sensor Hardware Design

VIIRS instrument was designed to collect radiometric and imaging data in twenty two (22) spectral bands covering the visible and infrared spectral region from 0.412 μm to 12.01 μm (Tables 1.a, 1.b).² The moderate resolution bands (M-bands) and imaging resolution bands (I-bands) have a spatial resolution of 740 m and 370 m respectively, while the ground swath is about 3040 km, permitting daily global coverage.

Table 1.a. VIIRS 15 reflective solar bands (RSB) characteristics and key requirements.

Reflective Solar Bands (RSB)									
Band Name	Gain	Center Wavelength (nm)	Bandwidth (nm)	FPA	FOV (km) Nadir/EOS	Polarization (%)	L_{TYP}	L_{MIN}/L_{MAX}	SNR
DNB	VG	700	400	DNB	0.8/1.6	NS	3 E-5 (*)	3e-5/200 (*)	6
M1	HG	412	20	VISNIR	0.8/1.6	3	44.9	30/135	352
	LG						155	135/615	316
M2	HG	445	18	VISNIR	0.8/1.6	2.5	40	26/127	380
	LG						146	127/687	409
M3	HG	488	20	VISNIR	0.8/1.6	2.5	32	22/107	416
	LG						123	107/702	414
M4	HG	555	20	VISNIR	0.8/1.6	2.5	21	12/78	362
	LG						90	78/667	315
M5	HG	672	20	VISNIR	0.8/1.6	2.5	10	8.6/59	242
	LG						68	59/651	360
I1	SG	640	80	VISNIR	0.4/0.8	2.5	22	5/718	119
M6	SG	746	15	VISNIR	0.8/1.6	2.5	9.6	5.3/41	199
M7	HG	865	39	VISNIR	0.8/1.6	3	6.4	3.4/29	215
	LG						33.4	29/349	340
I2	SG	865	39	VISNIR	0.4/0.8	3	25	10.3/349	150
M8	SG	1240	20	SMWIR	0.8/1.6	NS	5.4	3.5/164.9	74
M9	SG	1378	15	SMWIR	0.8/1.6	NS	6	0.6/77.1	83
M10	SG	1610	60	SMWIR	0.8/1.6	NS	7.3	1.2/71.2	342
I3	SG	1610	60	SMWIR	0.4/0.8	NS	7.3	1.2/72.5	6
M11	SG	2250	50	SMWIR	0.8/1.6	NS	0.12	0.12/31.8	10

Notes:

*: DNB units are in $\text{W}\cdot\text{cm}^{-2}\cdot\text{sr}^{-1}$

The units of spectral radiance for L_{TYP} , L_{MIN} and L_{MAX} are $\text{W}\cdot\text{m}^{-2}\cdot\text{sr}^{-1}\cdot\mu\text{m}^{-1}$

Dual-gain M-bands have two entries, one for high-gain (HG) and one for low-gain (LG)

VG: Variable Gain. DNB has three gains: high gain, mid gain, and low gain.

The SNR is the minimum (worse-case) required SNR that applies at the end-of-scan

EOS: End-of-Scan, FOV: Field of View

Table 1.b. VIIRS 7 thermal emissive bands (TEB) characteristics and key requirements.

Band Name	Gain	Center Wavelength (nm)	Bandwidth (nm)	Focal Plane Assembly	FOV (km) Nadir/EOS	Polarization Sensitivity (%)	T _{TYP} (K)	T _{MIN} /T _{MAX} (K)	NEdT (K)
I4	SG	3740	380	SMWIR	0.4/0.8	NS	270	210/353	2.5
M12	SG	3760	180	SMWIR	0.8/1.6	NS	270	230/353	0.396
M13	HG	4050	155	SMWIR	0.8/1.6	NS	300	230/343	0.107
	LG						380	343/634	0.423
M14	SG	8550	300	LWIR	0.8/1.6	NS	270	190/336	0.091
M15	SG	10763	1000	LWIR	0.8/1.6	NS	300	190/343	0.07
I5	SG	11450	1900	LWIR	0.4/0.8	NS	210	190/340	1.5
M16	SG	12013	950	LWIR	0.8/1.6	NS	300	190/340	0.072

Notes:

The NEdT is the maximum (worse-case) required NEdT that applies at the end-of-scan
 SG: Single Gain, NS: Not Specified, EOS: End-of-Scan, FOV: Field of View

The VIIRS sensor was partitioned into two major modules: the Opto-Mechanical Module and the Electronics Module. The Sensor has been designed so that each module is separately mounted onto the spacecraft as depicted in Figure 1. J1 VIIRS has the same design as SNPP VIIRS with similar on-board calibrators: the Spectralon® solar diffuser (SD) to calibrate the RSB, the solar diffuser stability monitor (SDSM) to track the SD spectral degradation, the V-groove blackbody (BB) to calibrate the TEB, and the space view (SV) to be used for background subtraction (Figure 1).

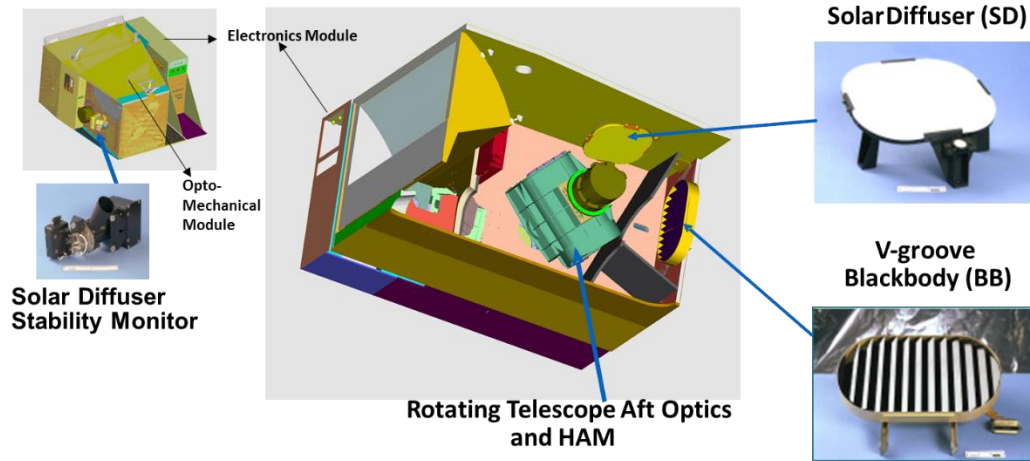


Figure 1. VIIRS instrument design and on-board calibrators: SD, SDSM, and BB.

VIIRS design has achieved multiple enhancements based on lessons learned from heritage sensors, including MODIS and SNPP.² VIIRS design is based on a rotating telescope that collects and distributes the light to three focal planes, the Visible Near-Infrared (VisNIR), the Short- and Mid-Wave Infrared (SMWIR), and the Long-Wave Infrared (LWIR). Bands located on the SMWIR and LWIR focal planes are thermally controlled at about 80.5 K. The VIIRS telescope scans in sequence the Earth within $\pm 56.1^\circ$ of nadir, then the blackbody (99.57° to 100.42°), the SD (158.57° to 159.42°), and then the SV (-66.10° to -65.25°).

2.2 Sensor Performance Testing

A comprehensive and intensive test program was completed to ensure high quality J1 VIIRS characterization and calibration. The test data collected provided a good understanding of the instrument performance, and allowed thorough investigation of sensor features and issues identified during testing. This successful test program is the result of an efficient collaboration between multiple government funded teams, including NASA, Aerospace Corp., NOAA, the University of Wisconsin, and the expertise provided by the sensor vendor, Raytheon. VIIRS general test plan covers two (2) key pre-launch phases: ambient (August 2013-January 2014) and thermal vacuum (TV) (July-October 2014), which allowed the collection of the calibration and characterization values needed for different bands, detectors, gain states, half angle mirror (HAM) sides, electronics configurations, and instrument temperatures. Key performance testing was conducted at three (3) instrument plateaus (Cold, Nominal and Hot) which were designed to cover the range of expected on-orbit conditions. J1 VIIRS key performance testing is described in Table 2.

Table 2: Key performance testing during Ambient and Thermal Vacuum testing phases.

Ambient Phase Testing 08/2013 - 01/2014	Thermal Vacuum Testing 07/2014 - 10/2014
Polarization Sensitivity	Reflective & Emissive Bands Calibration
Near Field Response (NFR)	Radiometric Stability
Stray Light Rejection (SLR)	Gain Transition Determination
Response Versus Scan (RVS)	Relative Spectral Response (RSR) in-band & OOB
Electrical and Dynamic Crosstalk	Band-to-Band Registration (BBR)
Radiometric Characterization: SNR, Gain	Line Spread Function (LSF)

Early in the J1 test program, four (4) important decisions were made that will define how the instrument will be operated: 1) replacing the VIIRS 1394 communication bus with the SpaceWire to resolve the anomalies observed by SNPP on-orbit³, 2) replacing the single board computer with a new design to resolve the computer lock-up issue observed by SNPP³, 3) setting the cold focal planes temperature at 80.5 K based on the thermal balance performed at TV hot plateau, 4) and designating the VIIRS electronics side A as the primary electronics, even though both sides showed comparable performance.

3. J1 VIIRS PRE-LAUNCH PERFORMANCE SUMMARY

This section will provide a summary of J1 VIIRS radiometric performance assessment based on the NASA VCST team test data analysis. Results will show the comparisons to the sensor specifications and to SNPP VIIRS performance. Methodologies used to generate performance are in general identical to those used for SNPP VIIRS².

3.1 Reflective solar bands (RSB) calibration

A National Institute of Standards and Technology (NIST) traceable light source, the 100 cm diameter Spherical Integrating Source (SIS100) was used during TV testing to characterize and calibrate the VIIRS RSB. Bands M1-M3 low gain were tested using another source, the Three Mirror Collimator (TMC) SIS, capable of reaching high radiance values. In addition, the space view source (SVS) was used to collect the dark offset needed to generate the background corrected detector response or digital number (dn).

The relationship between the detector response and the light source radiance L ($\text{Wm}^{-2} \text{sr}^{-1} \mu\text{m}^{-1}$) is represented by a polynomial equation:

$$L = c_0 + c_1 \cdot dn + c_2 \cdot dn^2 + O(dn^3), \quad (1)$$

where c_0 , c_1 , and c_2 are the calibration coefficients; $O(dn^3)$ denotes the truncation error.

The calibration coefficients were determined through curve fitting; however, the instability of the source over time and dynamic range [L_{\min} , L_{\max}] can lead to high uncertainties in the derived coefficients. To mitigate the impact of the source instability, the radiance measurements were performed with and without an attenuator screen inserted into the optical path. The attenuator screen is an opaque plate with small holes to allow the transmission of a fraction of the light. The time between attenuator in and out is very short to minimize the effect of source instability on the measurements (~2 minutes).

Consequently, the ratio of the detected spectral radiances with and without the attenuator is equal to the attenuator transmittance (τ), as ⁴:

$$\tau = \frac{c_0 / c_1 + dn_{in} + (c_2 / c_1)dn_{in}^2}{c_0 / c_1 + dn_{out} + (c_2 / c_1)dn_{out}^2}, \quad (2)$$

where dn_{in} and dn_{out} denote the dn with and without the attenuator, respectively.

To facilitate the data regression, Eq. (2) is rewritten as:

$$h_0(\tau - 1) + (\tau dn_{out} - dn_{in}) + h_2(\tau dn_{out}^2 - dn_{in}^2) = 0 \quad (3)$$

where $h_0 = c_0/c_1$, and $h_2 = c_2/c_1$

The model parameters τ , h_0 , and h_2 are determined through a non-linear least-squares fitting process, and the linear coefficient or gain is determined by inverting Eq. (1) and averaging over the selected source levels:

$$c_1 = \left\langle \frac{L}{h_0 + dn_{out} + h_2 dn_{out}^2} \right\rangle \quad (4)$$

In addition to a comprehensive set of RSB calibration coefficients that was generated for all sensor configurations, our findings have confirmed that all RSB have very good linearity, except the DNB and SWIR bands at very low radiances. J1 SWIR M-bands exhibited more non-linear behavior at low radiance than was observed on SNPP. Figure 2 shows the ratios of the attenuator out signal to the attenuator in signal for SWIR bands M8-M11. The root-cause of this issue was linked to an incorrect bias voltage for the SMWIR M-bands. This SWIR non-linearity led to larger than expected radiance characterization uncertainty and non-uniformity. A mitigation plan is being prepared to enhance the calibration performance of the SWIR bands.

Test data analysis also showed a larger than expected non-linear response for DNB high gain A and B (HGA, HGB). The mid-gain and low gain stages also showed non-linearity features, but to a much lower extent. Upon further analysis, linear fits showed increasing residuals for the high gain stages from aggregation modes 21 up to 32. The root cause of this DNB non-linearity issue was associated to two incorrect bias settings in the focal plane interface electronics.

Figure 3 shows the DNB response (dn) for HGB (HGA shows similar features) at three aggregation modes (1, 21 and 32), where the non-linearity is clearly increasing from aggregation mode 21 up to aggregation 32. This non-linearity also increases as the radiance decreases. This issue was intensively investigated, and a solution referenced as Option 21 was identified to significantly reduce the non-linearity effect, at the expense of increased spatial resolution (low risk).

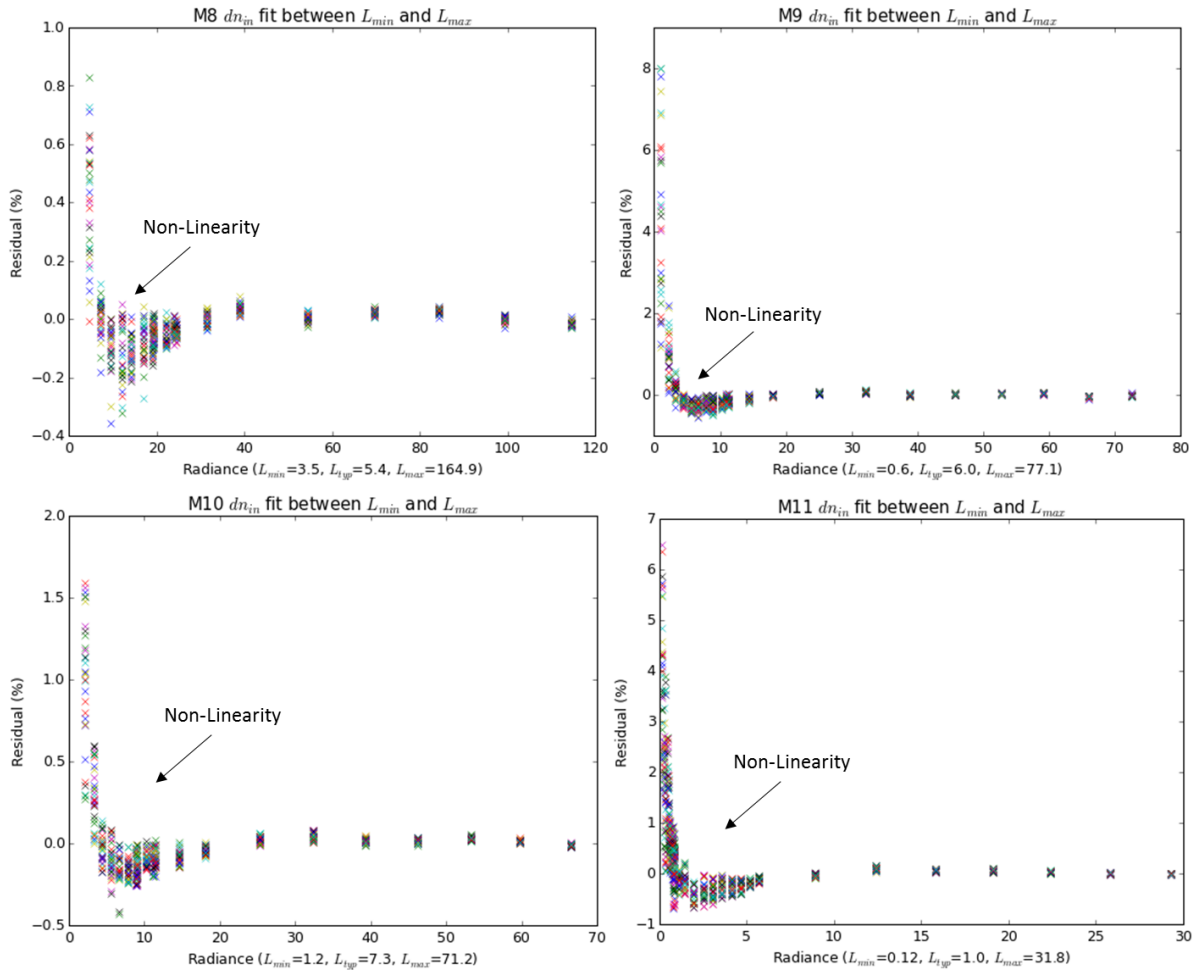


Figure 2: J1 SWIR non-linearity: ratio of sensor response value (dn) for attenuator in and out

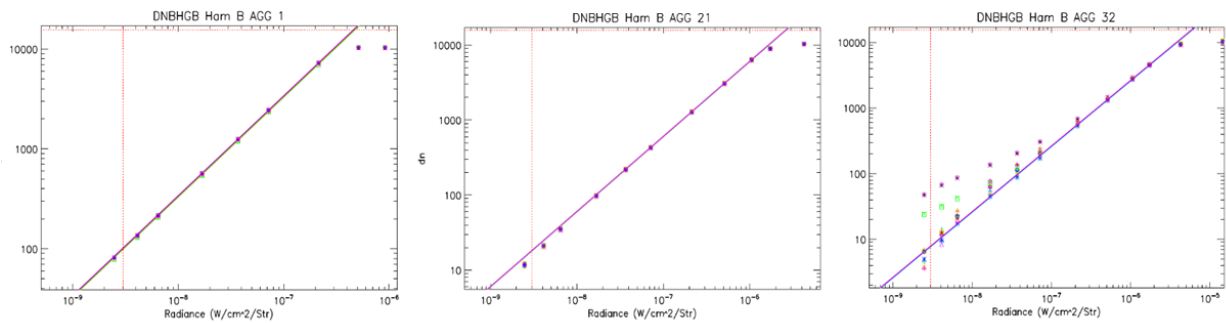


Figure 3: J1 DNB HGB response (dn) as a function of radiance in aggregation zones 1, 21 and 32. The non-linearity increases from aggregation mode 21 up to aggregation mode 32 at low radiance. The symbols represent the 16 DNB detectors.

SNR Calculation

The SNR was calculated for each RSB detector and for all SIS radiance levels. The SNR is calculated for each sample position to eliminate artifacts due to source non-uniformity, by dividing the sample averaged dn over scans by the standard deviation as:

$$SNR = \frac{1}{M} \sum_{j=1}^{j=M} \left[\frac{\frac{1}{N} \left[\sum_{i=1}^{i=N} dn_{i,j} \right]}{\sigma_j} \right] \quad (5)$$

where M, N are the total number of samples and scans respectively, and i, j are the scan and sample indices respectively. A mathematical equation was used to fit the SNR as a function of radiance to facilitate the computation of the SNR at any radiance level within the dynamic range:

$$SNR = \frac{L}{\sqrt{k_0 + k_1 L + k_2 L^2}} \quad (6)$$

The band averaged SNR and radiance saturation values are shown in Figure 4.a. All J1 RSB meet the SNR specification at L_{typ} with margins which are in general larger than those measured for SNPP. It is also worth noting that without the mirror coating contamination in the SNPP RTA, J1 SNR performance is expected to have even better margins than SNPP at the end of mission life. The smallest and largest SNR margins for J1 are 51% and 3172% for M2 (high gain) and I3, respectively. It is also worth mentioning that I3 detector 4 is a very noisy detector (not shown here), with a responsivity of about 50% less than the other detectors in this band.

RSB saturation is comparable to SNPP (Figure 4.b), meeting specification with acceptable margins, except for bands M8 (72%) and I3 (91%). These two L_{max} non-compliances were expected and have limited effect on science based on SNPP experience.

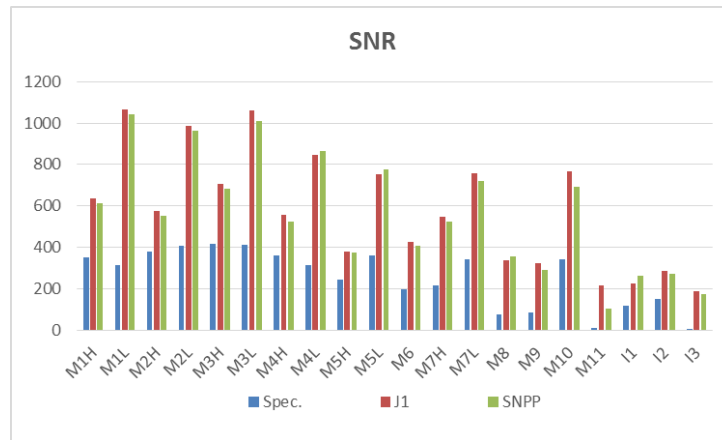


Figure 4.a: J1 VIIRS SNR values for RSB with comparison to both the specification and SNPP

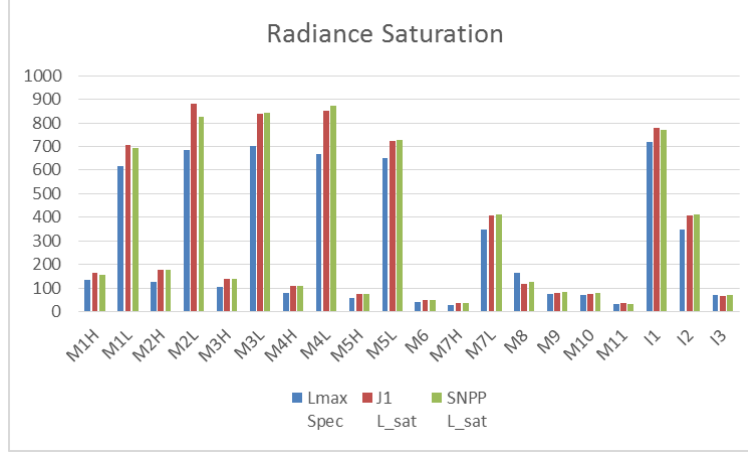


Figure 4.b: J1 VIIRS radiance saturation (L_{sat}) values for RSB with comparison to both the specification and SNPP

RSB radiometric calibration uncertainty

VIIRS RSB radiometric uncertainty requirement was set to 2% when viewing a uniform scene of typical radiance, L_{typ} . This calibration uncertainty verification was performed using contributors which have been constrained by sensor-level requirements while others are based on the sensor contractor allocations. The detector response characterization uncertainty is a key contributor to the overall uncertainty, which limit the calibration fitting error to less than 0.3%. This characterization uncertainty requirement was very challenging for the VIIRS RSB to meet, but the spectral reflectance accuracy (2%) was met for all RSB except M11 (2.25%),⁵ primarily due to the uncertainty of the SD bi-directional reflectance factor (BRF).

3.2 Thermal emissive bands (TEB) calibration

A NIST traceable external Blackbody Calibration Source (BCS) was used to calibrate J1 VIIRS thermal emissive bands. The radiance reaching the detector is the sum of the source radiance as well as emissions from RTA, HAM, and aft optics.

The path difference radiance between the two sources (BCS and SV) is written as:

$$\Delta L_{BCS} = RVS_{BCS} \epsilon_{BCS} L_{BCS} - \frac{(RVS_{BCS} - RVS_{SV})}{\rho_{RTA}} [L_{HAM} - (1 - \rho_{RTA}) L_{RTA}]. \quad (7)$$

The reflectance factors represent the total reflectance of the RTA mirrors and aft-optics. The RVS is the scan angle dependent, relative reflectance of the HAM. The radiances of the sources are determined via Planck's law convolved over the relative spectral response (RSR) of each spectral band over the extended band pass. Thermistors located inside the sensor were used to determine the temperature of each source.

A quadratic polynomial in the offset corrected digital response (dn) is used to calculate the path difference at-detector radiance:

$$\Delta L = c_0 + c_1 dn + c_2 dn^2. \quad (8)$$

By inverting Eq. (8) we were able to retrieved EV radiance for the BCS:

$$L_{BCS-ret} = \frac{(c_0 + c_1 dn_{BCS} + c_2 dn_{BCS}^2)}{RVS_{BCS}} + \frac{(RVS_{BCS} - RVS_{SV})}{RVS_{BCS} \rho_{RTA}} [L_{HAM} - (1 - \rho_{RTA}) L_{RTA}]. \quad (9)$$

Both the BCS and OBCBB were transitioned through a series of temperature levels; the data acquired was used to determine the coefficients by fitting the path difference radiance versus the detector response within the dynamic range. A high temperature external blackbody (TMC BB) was used to calibrate the low gain state of band M13, and the calibration of the TMC BB was tied to the BCS at lower scene temperatures where both sources overlap.

NEdT calculation

The noise equivalent differential temperature (NEdT) is the fluctuation in the scene temperature equivalent to the system noise and is computed via the equation

$$NEdT = \frac{\Delta L_{BCS}}{SNR \frac{\partial L}{\partial T}} \quad (10)$$

The NEdT was determined at all source levels and compared to the specified value at T_{TYP} ; this was determined using the fit SNR and at-detector radiance. The band average NEdT results are below specification as shown in figure 5.a. All emissive bands and detectors meet the NEdT specification with good margins, and performance is comparable to SNPP. The smallest and greatest margins were observed for M14 (39%) and I4 (595%) respectively. Detector variability is small in general, with the exception of detector 4 in M15 and detector 5 in M16B which are out-of-family detectors.

Figure 5.b shows the J1 maximum temperature and comparison to L_{max} specification and SNPP. All bands have saturation values above the specified L_{max} , and comparable to SNPP. M13 low gain saturation was not observed in TV testing, but saturation is expected to be around 670 K based on ambient testing.

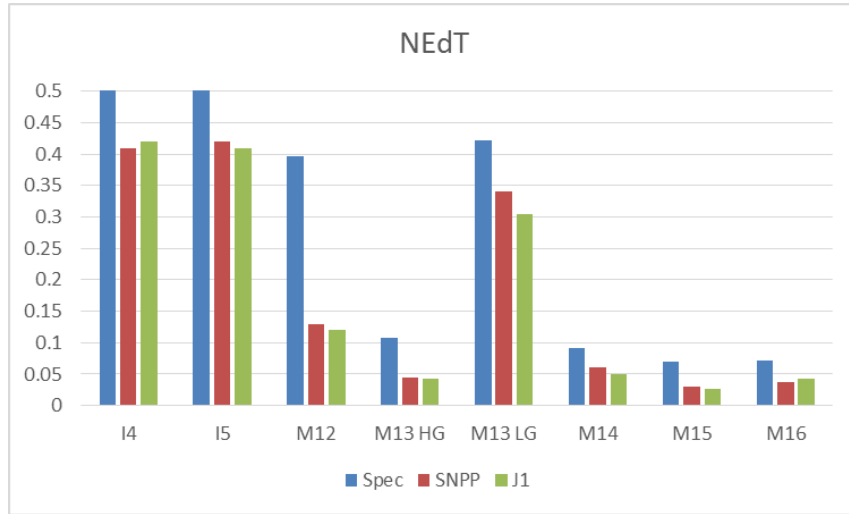


Figure 5.a: J1 VIIRS NEdT (K) performance for TEB (the specification for I4 and I5 is 2.5 and 1.5 respectively, but were limited to 0.5 for clarity in the plot)

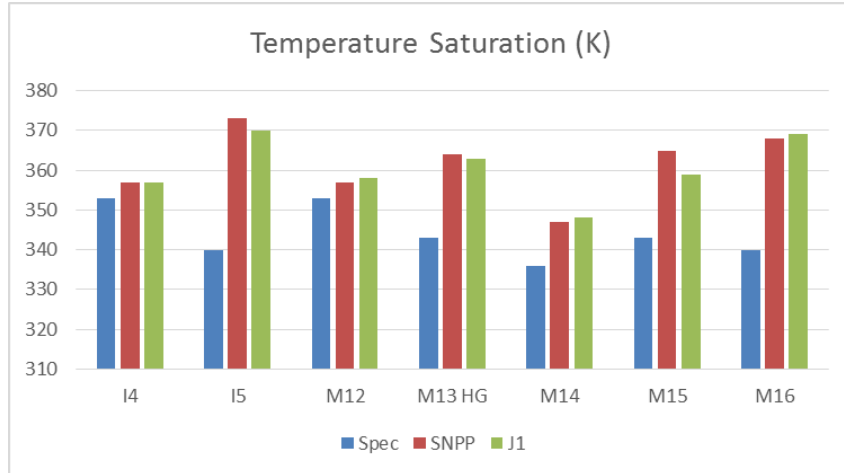


Figure 5.b: J1 VIIRS temperature saturation for TEB

Figure 6 shows the detector-to-detector striping represented by the relative radiometric uniformity (RRU) metric:

$$RRU = \frac{|L_{BCS-ret} - \langle L_{BCS-ret} \rangle_D|}{NE\Delta L}, \quad (11)$$

RRU values larger than one mean that the sensor is not compliant with detector striping requirements. The risk of striping increases with temperature for all TEB bands. Results derived per HAM side, electronics side and temperature plateau have shown some performance variations, with RRU for some bands reaching up to 1.8 at the highest temperatures. This requirement was difficult to meet for both SNPP and J1 since VIIRS TEB has very good noise performance.

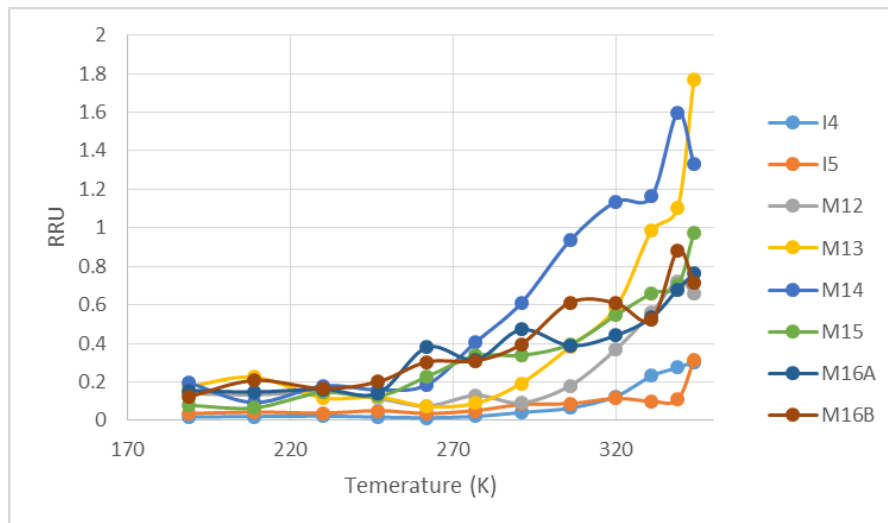


Figure 6: J1 maximum RRU as a function of source (BCS) temperature is shown for all TEB, for electronics side A, HAM B, and Nominal plateau.

The percent difference between the retrieved and BCS radiances is represented by the Absolute Radiance Difference (ARD), and it is essentially a measure of the fitting uncertainty:

$$ARD = 100 \frac{L_{BCS-ret} - L_{BCS}}{L_{BCS}} \quad (12)$$

The band averaged ARD for J1 TEB derived at Nominal plateau, electronics side A are shown in Table 3 alongside the specified values in the lower part of the table. As expected, the ARD results show excellent thermal calibration for all bands at the specified temperatures, and the only exception is M12 at very low temperature (230 K) where the ARD value of 7.6 is slightly higher than the specified value of 7.0. Again, the ARD performance is comparable between J1 and SNPP.

Table 3: TEB band averaged ARD at specified temperature, for electronics side A, HAM A, and Nominal plateau.

ARD Performance (%)								
Temp (K)	I4	I5	M12	M13	M14	M15	M16A	M16B
190	~	~	~	~	0.68	0.29	0.17	0.25
230	~	~	7.60	2.95	0.11	0.07	0.08	0.04
267	0.48	0.10	~	~	~	~	~	~
270	~	~	0.24	0.15	0.08	0.05	0.04	0.04
310	~	~	0.25	0.17	0.11	0.06	0.03	0.04
340	~	~	0.27	0.18	0.09	0.05	0.03	0.03
ARD Specification (%)								
Temp (K)	I4	I5	M12	M13	M14	M15	M16A	M16B
190	~	~	~	~	12.30	2.10	1.60	1.60
230	~	~	7.00	5.70	2.40	0.60	0.60	0.60
267	5.00	2.50	~	~	~	~	~	~
270	~	~	0.70	0.70	0.60	0.40	0.40	0.40
310	~	~	0.70	0.70	0.40	0.40	0.40	0.40
340	~	~	0.70	0.70	0.50	0.40	0.40	0.40

3.3 Other Performance Testing

Polarization

J1 polarization sensitivity was characterized in ambient testing using an integrating sphere combined with a sheet polarizer at seven different scan angles in the 400 to 900 nm range^{6,7}. The sheet polarizer was mounted on a rotary stage and was rotated in 15 degree increments from 0 to 360 degrees. The polarization sensitivity was derived for all VisNIR bands, detectors, HAM sides, and seven scan angles (-55, -45, -22, -8, 20, 45, 55), using a Fourier series. The polarization sensitivity measurements were of good quality, however, the polarization factors for bands M1-M4 have revealed unexpectedly large non-compliance. The root cause of these non-compliances was the redesigned VisNIR spectral filters, and confirmed by the sensor polarization model^{6,7}. Additional polarization testing was executed in the post-TV phase for more scan angles (-37, -30, -15, 4) and limited testing with a laser source for two bands, M1 and M4, to verify the quality of the sensor polarization modeling⁶.

Table 4 shows the final J1 mean polarization factors for all VisNIR bands (HAM A). The linear polarization sensitivity for bands M1 – M4 was observed to be higher than the specified limit, with maximums as high as ~6.42 % for M1, ~4.36 % for M2, ~3.08 % for M3, and ~4.35 % for M4. A difference between HAM sides was also seen, reaching up to 1 %. Furthermore, quite large detector-to-detector and scan angle differences were observed within bands, up to ~4 % in M1. The polarization performance from ambient phase was confirmed using special testing during post-TV phase, and indicated that the sensor polarization model predictions are acceptable but the model needs enhancement, especially for band M4.

Table 4: Overview of VisNIR linear polarization factor for both J1 and SNPP sensors, for HAM side A. Numbers in bold represent performance non-compliance ($-45 < \text{scan angle} < +45$)

Band	Sensor	Scan Angle										Max Pol.	Spec	
		-55	-45	-37	-30	-22	-15	-8	4	20	45			55
I1	SNPP	0.86	0.76	-	-	0.62	-	0.59	-	0.54	0.58	0.61	1.24	2.5
	J1	0.86	0.9	0.95	0.95	0.94	0.98	0.95	0.98	1	1.03	1.04	1.03	2.5
I2	SNPP	0.49	0.45	-	-	0.47	-	0.51	-	0.56	0.56	0.55	0.56	3
	J1	1.19	0.92	0.75	0.62	0.5	0.51	0.48	0.5	0.53	0.58	0.61	0.92	3
M1	SNPP	3.14	2.73	-	-	2.01	-	1.83	-	1.45	1.23	1.39	2.73	3
	J1	5.57	5.73	5.86	6.06	6.17	6.19	6.34	6.41	6.42	6.17	5.96	6.42	3
M2	SNPP	2.25	2.05	-	-	1.65	-	1.54	-	1.28	1.17	1.3	2.05	2.5
	J1	4.08	4.08	4.13	4.23	4.18	4.18	4.23	4.25	4.19	4.36	4.46	4.36	2.5
M3	SNPP	1.45	1.31	-	-	0.96	-	0.85	-	0.62	0.71	0.81	1.31	2.5
	J1	2.92	2.86	2.83	2.85	2.76	2.74	2.75	2.74	2.85	3.08	3.11	3.08	2.5
M4	SNPP	1.59	1.52	-	-	1.37	-	1.3	-	1.02	0.86	0.82	1.52	2.5
	J1	4.03	4.2	4.33	4.35	4.32	4.35	4.3	4.29	4.15	3.99	3.91	4.35	2.5
M5	SNPP	0.81	0.74	-	-	0.7	-	0.69	-	0.61	0.59	0.57	1.02	2.5
	J1	2.1	2.17	2.23	2.19	2.13	2.14	2.07	2.03	2.02	1.99	1.97	2.23	2.5
M6	SNPP	1.29	1.14	-	-	0.96	-	0.92	-	0.81	0.75	0.7	1.14	2.5
	J1	1.03	0.92	0.89	0.87	0.86	0.91	0.91	0.95	0.96	0.95	0.94	1.32	2.5
M7	SNPP	0.52	0.47	-	-	0.43	-	0.44	-	0.48	0.47	0.45	0.48	3
	J1	1.18	0.92	0.74	0.61	0.48	0.47	0.43	0.46	0.47	0.52	0.56	0.92	3

Relative Spectral Response

The RSR of the VisNIR bands were measured under ambient conditions while the RSR of SMWIR and LWIR was measured in the TV environment at Nominal plateau ⁸. While the main J1 spectral testing was based on a monochromator source, a laser source was used in the post-TV phase to collect additional VisNIR RSR data. This spectral testing led to high quality J1 spectral characterization. Figure 7 shows the in-band response for all VIIRS RSB and TEB based on a combination of best quality measurements from the monochromator and the laser sources. When compared to SNPP, the spectral testing has shown good enhancement of J1 RSR performance, such as OOB reduction, especially for band M1 (figure 8). Compliance with the band center, bandwidth, extended band pass, and Integrated OOB (IOOB) requirements were calculated for all bands on a per detector basis. Only few non-compliances were identified and are either similar to SNPP or considered a low risk for VIIRS products.

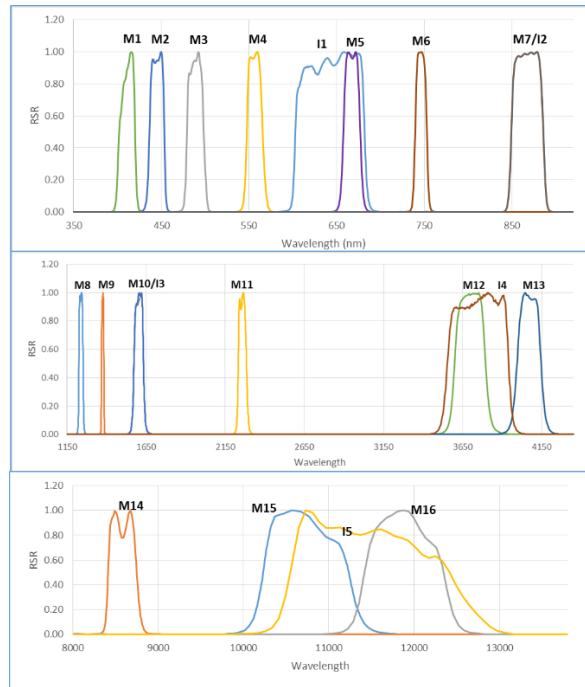


Figure 7: J1 VIIRS RSR (in-band) for all RSB and TEB

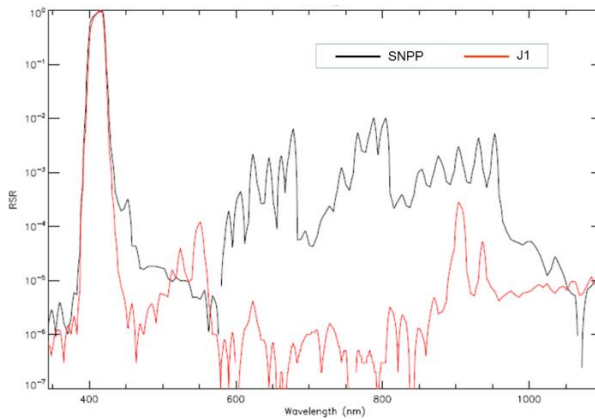


Figure 8: The J1 M1 full RSR (in-band and OOB), and comparison with SNPP

Response Versus Scan Angle

RSB RVS was measured using the SIS-100 and for the TEB using a cavity type blackbody and the on-board BB. Data taken at eleven angles-of-incidence (AOI) for RSB and twelve for TEB were used to fit the RVS function, which is a quadratic polynomial in AOI, after corrections for source drift and background radiances were performed⁹. J1 band-average RVS as a function for HAM AOI (HAM A and B) is shown on Figure 9. The RVS differences between HAM sides are small with the exception of bands M1, M2, M7 and I2. The variation in the RSB RVS is less than 1.5 % and similar to SNPP. M1 has the largest variation over the full operational AOI range of 28.6° to 60.2°. The uncertainty of RSB RVS was about 0.2 % (less than the target of 0.3 %) which was determined as the average fitting residuals. The MWIR RVS is generally small varying by less than 1 % over the full AOI range. In contrast, the LWIR RVS changes by up to 10 % for M14 over the range of AOI. The uncertainty of the TEB RVS was less than 0.1 %, and meet the uncertainty target of 0.2 %. Overall, J1 RVS performance is comparable to SNPP performance.

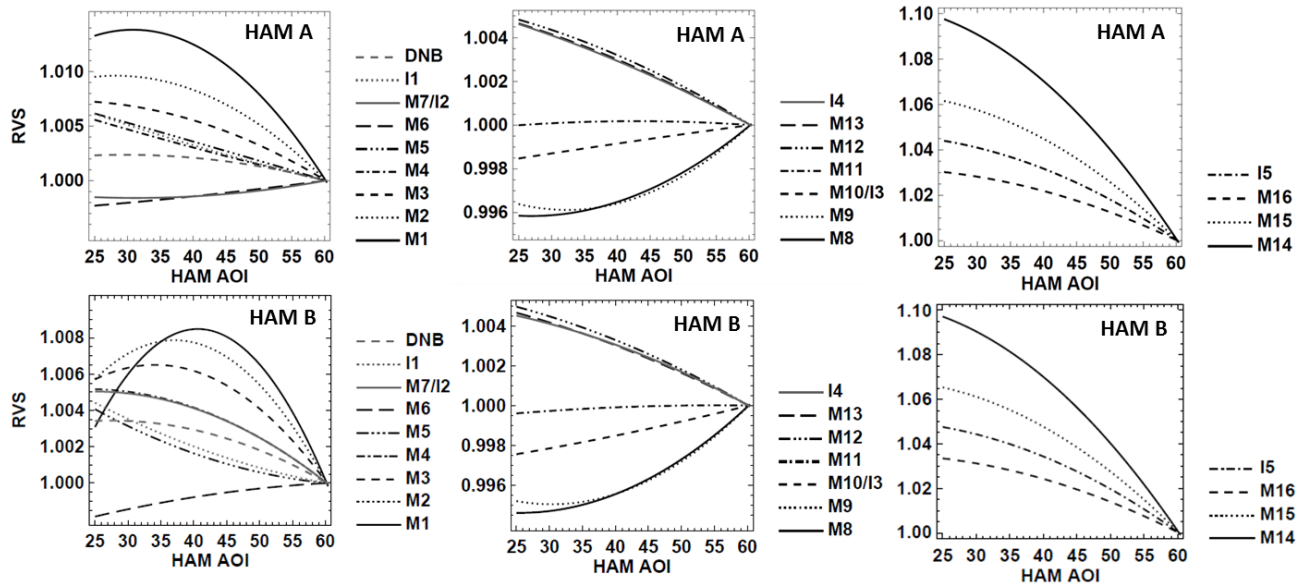


Figure 9: The RVS (HAM A and B) of J1 VIIRS bands as a function AOI

Near Field Response

The scattered light performance is crucial to well calibrated instruments. Near field response (NFR) testing measures the scattered light originating from within 4 degrees from the RTA line of sight using a light source called the Scatter Measurement Assembly (ScMA). This testing was used to verify the VIIRS NFR requirement defined as the maximum allowable response at a specified angle limit coming off a 20 by 20 km bright target for each band. A Harvey-Shack BRDF scattering model was used to fit the measured NFR profile and remove test artifacts and noisy samples.

Figure 10 shows the normalized response for band M5 detector 8 (SNPP and J1) which represents a typical profile observed in the VIIRS NFR measurements when the sensor is scanning the source through a vertical slit reticle. For both SNPP and J1, the figure shows the NFR falling off rapidly from the peak with additional sharp drops observed around the field baffle locations. The NFR is estimated for each detector, and the results show good detector uniformity within the same band. The J1 band averaged NFR performance is compliant for all bands (Figure 11), and is in general better than SNPP.

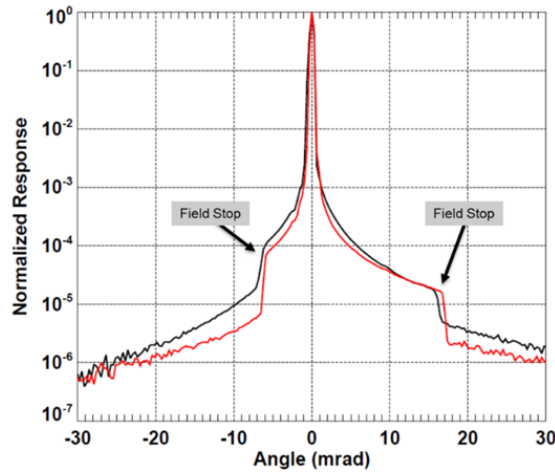


Figure 10: J1 Measured NFR for band M5 (672 nm) detector 8 (red line), and comparison to SNPP (black line).

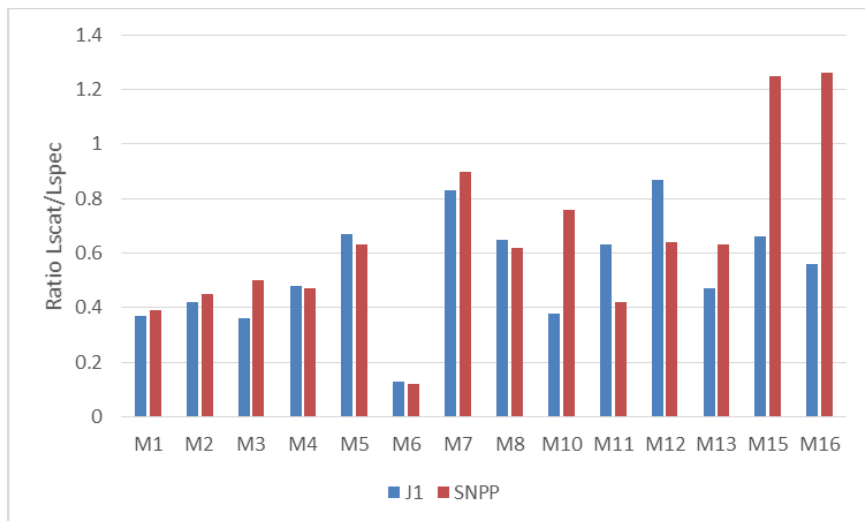


Figure 11: Summary of J1 VIIRS NFR performance. Compliance is met when the ratio of scattered light (L_{scat}) to requirement (L_{spec}) is less than 1.

Stray Light Response

The far field stray light is part of the family of scattered light, and is defined as light originating from a region between 4 and 62.5 degrees from the sensor boresight. It was tested using a bright source (1000-W lamp). The VIIRS telescope was staring at a cavity type blackbody while the lamp was moved through 33 equal-distanced hemispherical positions, covering roughly equally divided annulus out to 62.5 degrees off nadir, and the measured instrument response was scaled by the ratio of the bright source irradiance and a model of bright cloud irradiance. The measured instrument response at each position was weighted by the corresponding annulus then aggregated to estimate the total stray light. The test was conducted with the RTA locked at SV, nadir, and end of scan to obtain stray light estimates at different scan angles.

The ratio between the band-averaged stray light and specification is shown on Figure 12. All RSB meet the stray light requirement with large margins at the beginning of life. Margins are between 50 % (M5) and 95 % (I3). Furthermore, test results indicate that J1 RSB stray light rejection is in general slightly better than SNPP. A noticeable difference is that the stray light in SNPP is much stronger along track than along scan direction; whereas in J1, the stray light is more evenly distributed in all angles. Another difference is that band M11 is now compliant for J1 because of the L_{typ} requirement change (from 0.1 to 1.0).

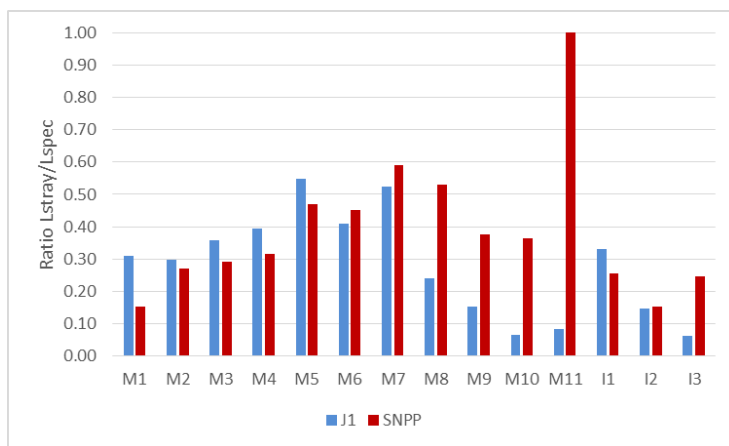


Figure 12: Summary of J1 VIIRS stray light performance. The ratio of measured stray light to requirement (1% L_{typ}) is less than 1 (i.e. requirement compliance). Symbols represent 16 detectors.

4. CONCLUSION

This paper provides an overview J1 VIIRS pre-launch radiometric performance, based on a comprehensive test program that was designed by the sensor contractor with support from the government calibration and science teams. The instrument test program was performed to characterize the radiometric, spectral and spatial performance for all 22 spectral bands in various configurations and environments, and simulating the range of on-orbit conditions (ambient and thermal vacuum). The VIIRS spectral bands calibration and characterization have shown very good performance, providing good quality calibration data to understand the instrument performance and to populate the SDR LUTs. The RSB SNR was compliant for all bands with minimum margin of 51% (M2) and maximum margin of 3172% (I3), while the dynamic range was compliant for all RSB except bands M8 (72%) and I3 (91%). As expected, and similar to SNPP, the TEB have shown very good performance in term of NEdT and dynamic range (full compliance). The spectral testing also provided high quality data to generate launch-ready sensor RSRs. All of the spectral non-compliances are expected to have negligible impact on the data products. The RVS derived for J1 was as expected, very similar to SNPP, and met the uncertainty target of 0.3% for RSB and 0.2% for TEB. The scattered light performance represented by the NFR and SLR met the sensor requirements for all bands, and are expected to lead to better or similar performance as SNPP. Overall, J1 performance was comparable to SNPP VIIRS, and it is expected to have high quality J1 data product post-launch. Two minor issues related to high

polarization sensitivity (M1–M4) and high non-linearity at low radiance for the DNB and SWIR bands were well characterized, and necessary mitigation plans are being prepared within the ground processing system to generate high quality products on-orbit.

Acknowledgments

The authors of this paper would like to thank the VIIRS team members from NOAA, Aerospace Corporation, NASA Science Team, University of Wisconsin and Raytheon for their valuable contributions to VIIRS testing and performance verifications. We also want to thank Jim McCarthy from Stellar Solutions and Chris Moeller from University of Wisconsin for their valuable discussions and contributions to enhance our understanding of VIIRS performance.

References

- [1] Lottman, B. T., Mussetto, M. S., McCarthy, J. K., Emch, P. G., Shipley, S. T., St. Germain, K., Mango, S. A., and Guenther, B. W., "NPP/NPOESS Joint Government SSPR Contractor Calibration and Validation program: system perspective, cooperative strategy and path to NPP", Proc. SPIE 5549, 20 (2004).
- [2] Oudrari, H., McIntire, J., Xiong, X., Butler, J., Lee, S., Lei, N., Schwarting, T., and Sun, J., "Pre-launch Radiometric Characterization and Calibration of the S-NPP VIIRS Sensor," IEEE T. Geosci. Remote, 53, 4, 2195-2210, (2015).
- [3] Xiong, X., Oudrari, H., Chiang, K., McIntire, J., Fulbright, J., Lei, N., Sun, J., Efremova, B., Wang, Z., and Butler, J., "VIIRS on-orbit calibration activities and performance", pp. 520 - 523, DOI: 10.1109/IGARSS.2013.6721207
- [4] Oudrari, H., McIntire, J., Xiong, X., Ji, Q., T. Schwarting, Lee, S. and Efremova, B., "JPSS-1 VIIRS Pre-Launch Radiometric Performance", Remote Sens. 2016, 8, 41; doi:10.3390/rs8010041.
- [5] Joint Polar Satellite System (JPSS) VIIRS Reflective Solar Bands - Performance Verification Report (PVR), Goddard Space Flight Center, Greenbelt, MD, USA, 2015.
- [6] McIntire, J., Young, J. B., Moyer, D., Waluschka, E., Oudrari, H., and Xiong, X., "Analysis of JPSS J1 VIIRS Polarization Sensitivity Using the NIST T-SIRCUS", Proc. SPIE. 9607, Earth Observing Systems XX, 96072D, 2015.
- [7] Waluschka, E., McCorkel, J., McIntire, J., Moyer, D., McAndrew, B., Brown, S.W., Lykke, K., Young, J. B., Fest, E., Butler, J., Wang, T.R., Monroy, E. O., Turpie, K., Meister, G., and Thome, K. J., "J1 VIIRS polarization narrative: testing and performance", Proc. SPIE 2015, 9607, 960712.
- [8] Moeller, C.; Schwarting, T.; McIntire, J.; Moyer, D. JPSS-1 VIIRS pre-launch spectral characterization and performance. Proc. SPIE 2015, 9607, 960711.
- [9] Moyer, D., McIntire, J., Oudrari, H., McCarthy, J., De Luccia, F., "JPSS1 reflectance versus scan angle (RVS) performance", Remote Sens. 2016, 8, 141; doi:10.3390/rs8020141.